

Land Degradation Assessment using Hyperspectral Imagery in Savanna Environment

Ramesh Bhatta
Rochester Institute of Technology

Abstract—Land degradation threatens ecosystem resilience, especially in regions affected by human-induced environmental alterations. Hyperspectral remote sensing offers a high-fidelity and data-abundant method in evaluating vegetation health and land cover dynamics to determine the status of land degradation. This study leverages hyperspectral imagery obtained from the Carnegie Airborne Observatory to assess land degradation by comparing conserved (Kruger National Park) and degraded (communal lands) regions in South Africa. The dataset spanning 24 bands from the visible (394.3 nm) to near-infrared (1044.9 nm) range was processed using the Spectral Hourglass Wizard in ENVI, involving Minimum Noise Fraction (MNF) transformation for dimensionality reduction, Pixel Purity Index (PPI) for end-member selection, and classification using Spectral Angle Mapper (SAM) and linear unmixing techniques. Four dominant land cover types—Photosynthetic Vegetation (PV), Non-photosynthetic Vegetation (NPV), Bare Soil (BS), and Shadow area (S)—were detected. Results highlight significant vegetation depletion in communal lands, with PV primarily concentrated along water sources, whereas the conserved region exhibits a more uniform distribution. The decline in NPV and increase in Bare Soil indicated land degradation due to the disruption of carbon and nutrient cycles. Classification accuracy assessment using stratified sampling (10 samples per class) demonstrated high accuracy for PV (90%–100% producer's accuracy, PA), while BS and S classes achieved 100% user's accuracy (UA). NPV posed the greatest classification challenge, showing misclassification with PV (UA: 72.73%). These findings highlight the ability of hyperspectral imaging in identifying and monitoring vegetation stress and land degradation, providing a useful insights for conservation planning and eco-friendly land management.

Index Terms—Land degradation, Hyperspectral remote sensing, Classification, Minimum Noise Fraction, Spectral Angle Mapper.

I. INTRODUCTION

LAND degradation is a crucial environmental challenge, mainly in areas affected by human-induced alterations due to deforestation, cattle grazing, agriculture, mining etc. as well as natural alterations due to bush encroachments, soil erosion, flooding. It disturbs ecosystem functions, resulting in reduced vegetation cover, soil degradation, and loss of biodiversity. Tracking these changes is important for effective land management and conservation efforts. Remote sensing provides a feasible tool for assessing land covers in such areas to differentiate and quantify between vegetation types, soil conditions and other indicators of land degradation. Such differentiation and quantification can be done by first determining the potential indicators of land degradation and classifying the whole area of interest into those indicators and use the classification result in identifying the extent of each indicators to establish the relationship between indicators and land

degradation. *Ashner et. al.* [1] demonstrated that indicators like Photosynthetic vegetation (PV), non-photosynthetic vegetation (NPV) and baresoil (BS) can reveal the condition of land in arid and semiarid lands. These vital indicators can be extracted by subsetting the available unique pixels (known as endmembers) present in the imagery data into a few endmembers based on the knowledge of the scene as well as the task we intend to perform. Various methods have been developed to determine endmembers (pure pixels) in a hyperspectral imagery [2]. *Pixel purity index* [3] is one of the most widely used methods which determines spectrally pure pixels in the scene by repeatedly projecting pixel spectra onto random unit vectors and recording extreme values. Pixels that frequently appear as extrema across multiple projections receive higher PPI scores, indicating their purity. After determining the endmembers spectra, the whole hyperspectral imagery can be expressed as the linear mixture of those unique spectra. This process is called *pixel unmixing* [4] and is generally used to determine the fraction unique pixels in the hyperspectral imagery. These fraction maps are called *abundance maps* as they represent the amount of each endmember in a pixel. These abundance map can be used to quantify the amount of each endmembers (indicators) present in the scene, which can show the level of land degradation in the region. Another way is to use these indicators and use their unique spectra to classify the whole scene. Hyperspectral imagery based classification shows a huge potential due to its ability to record the spectral response from each pixels using continuous narrow bands with high sampling and spectral resolution. Such detailed information from hyperspectral data allows for the distinction of minute spectral variations among the target of interest.

The huge amount of band information present in the hyperspectral data poses a problem that increase in band data increases the number of required training samples exponentially for maintaining classification accuracy [5]. This requires for using a suitable dimensionality reduction techniques for training of classification algorithm. One common technique for band data reduction in hyperspectral imagery for classification is *Minimum Noise Fraction (MNF)* [6]. The Minimum Noise Fraction (MNF) transformation is a two-step process involving *principal component analysis (PCA)*. First, it applies PCA to reduce correlations in noisy data, effectively separating noise from the signal. Then, the denoised principal components are used to perform the final transformation, enhancing the representation of essential image features. The MNF transformed bands are now ranked based on their importance/variability determined by the eigen-values from highest to lowest. These

MNF bands can be subsetted to few bands for training a classifier since higher bands generally represent noise. We used a simple yet elegant unsupervised classification method namely: *Spectral Angle Mapper (SAM)* [7] towards fulfilling our objectives: 1) Classification of conserved and degraded land regions into PV, NPV, BS and other important indicators and 2) Determine the level of land degradation in two regions based on classification outcomes and 3) Perform rudimentary accuracy assessment based on image interpretation of the hyperspectral scenes. The ideal application of this work is to leverage airborne hyperspectral remote sensing methods to analyze vegetation and soil conditions covering large area and provide insights into the extent of land degradation. Such results can guide conservation strategies and sustainable land management practices.

II. DATA AND METHODS

The data used in this task are two hyperspectral imagery collected by Carnegie Airborne Observatory (CAO)- one from *Kruger National Park (Landuse 2; conserved)* and another from the communal areas outside the park (*Landuse 7; degraded*), in South Africa as shown in Figure 1. The figure shows the distribution of vegetation is dense and concentrated to smaller area of whole scene in the conserved area (b) while most of the communal land is washed out and contains sparse vegetation across the scene with clearly visible human partitioned land areas (a).

The HSI data consists of 24 bands ranging from VIS (394.3 nm) to NIR region (1044.9 nm). We used ENVI's **Spectral Hourglass Wizard** to unmix the HSI imagery into unique pixels- *Photosynthetic Vegetation (PV)*, *Non-photosynthetic Vegetation (NPV)*, *Bare Soil (BS)* and *Shadow (S)* pixels. The way this routine works is that, first it takes the hyperspectral imagery and then dimensionality reduction is performed using the *Minimum Noise Fraction (MNF)* transform, which helps to project the original dataset to smaller number of MNF bands and also remove the noise from data which generally appear in higher MNF bands. After this, the *Pixel Purity Index (PPI)* calculation is applied to identify spectrally pure pixels by iteratively projecting data onto random unit vectors and logging the most extreme spectral responses. These potential end-members are then analyzed in the *n-Dimensional Visualizer*, an interactive tool that allows users to manually cluster and select pure spectral pixels or use the automatically detected clusters based on accuracy requirement. Since we are trying to detect 4 completely different types of spectral signatures the automatically detected clusters satisfied our requirement. Usually the PPI based endmembers detection gives us more than required number of endmembers and we need to select the endmembers which we are most interested in. Finally, the selected endmembers were used to generate abundance maps for each unique class using *linear unmixing* and also a classification map using *Spectral Angle Mapper (SAM)* dividing whole imagery into the desired classes. This classified map was then processed to remove *salt-and-pepper noise* and improve the spatial coherence of classified images using kernel based *Majority-Minority* smoothing. This method helps

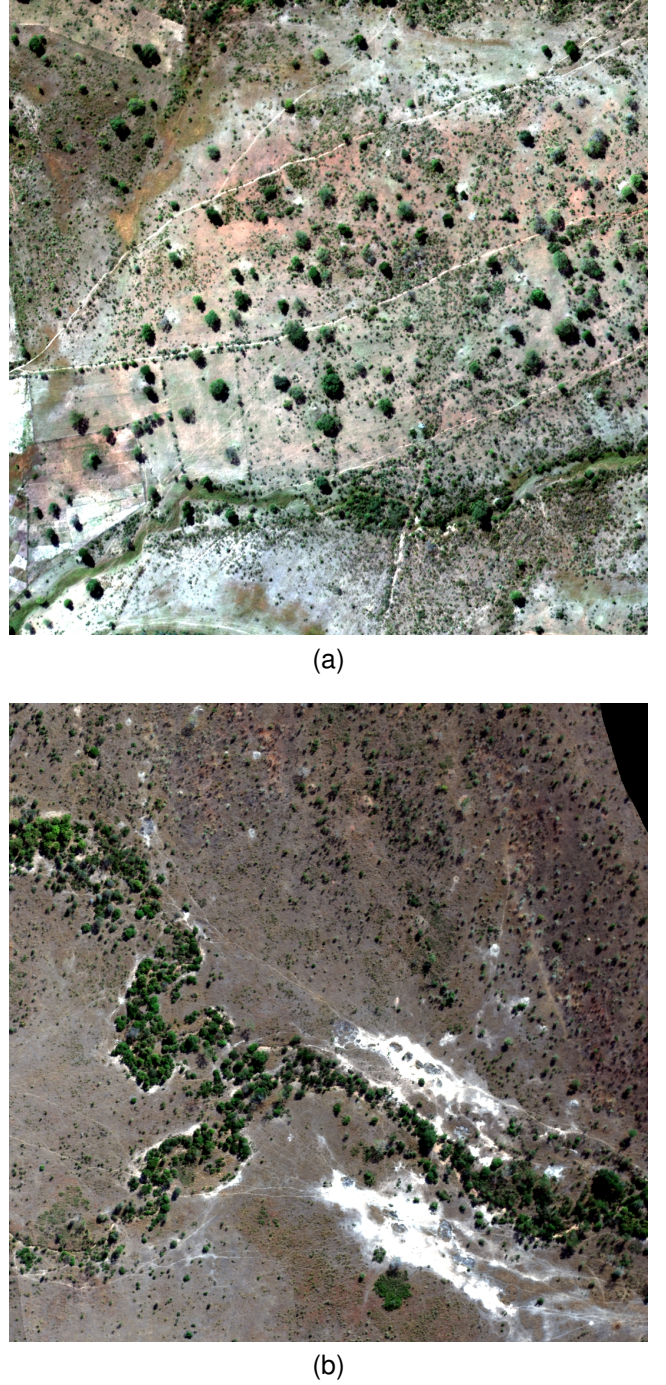


Fig. 1: Study Area- (a) Degraded Land, Landuse 7 and (b) Conserved Land, Kruger National Park, Landuse 2.

remove small, isolated classified regions (minority classes) and reinforces dominant classified regions (majority classes), making the classification results more visually and analytically meaningful. The algorithm examines the class labels of surrounding pixels within a specified window (e.g., 3×3 or 5×5). If a pixel belongs to a minority class within that window it is reassigned to the majority class. In this way classified map for each landuse case were obtained and finally their accuracy assessment was done based on [8].

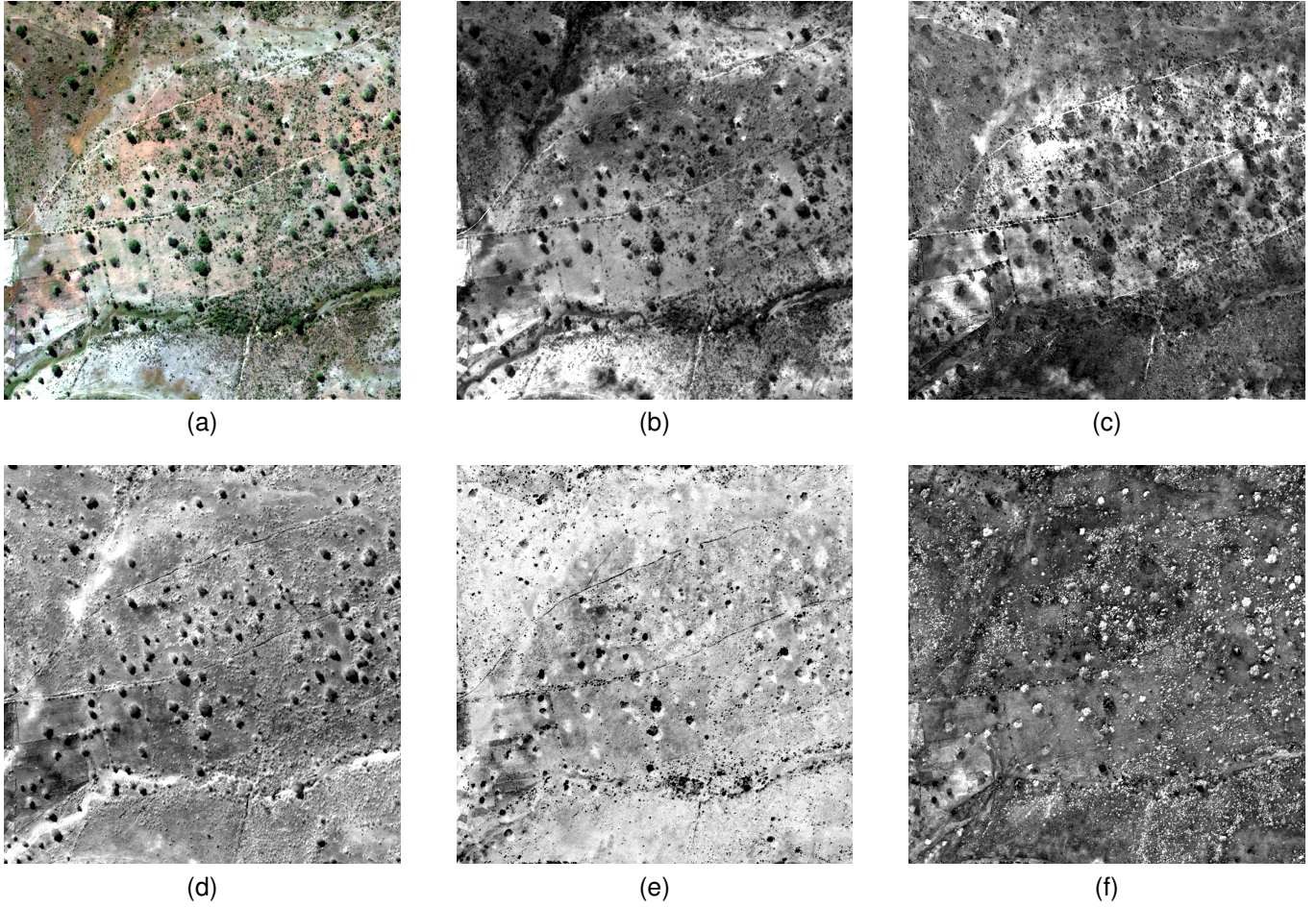


Fig. 2: First 5 MNF bands: (a) Original RGB Image (Landuse-7), (b) MNF B1, (c) MNF B2, (d) MNF B3, (e) MNF B4, and (f) MNF B5.

III. RESULTS

The result for minimum noise fraction (MNF) in Landuse-7 data is shown in Figure 2. We can see from the figure that the different MNF bands show variability in different features. For example MNF band 1 highlights Bare Soil areas, Band 2 looks like Non-photosynthetic vegetation areas, Band 3 highlights shadows and darker area in the image, Band 4 highlight the topographical variation and Band 5 highlights the healthy vegetation pixels. If features of interest is found in one of the PC bands we might not need to use other information for the analysis and hence MNF make the analysis more efficient and robust.

To choose how many of such bands we will use for the further analysis we used the graph of *Eigen value number* vs *Eigenvalue* as shown in Figure 3.

From the plot we can see that the curve for eigenvalue (Y-axis) decreases exponentially as we include more MNF bands (x-axis) and with about 10 MNF almost total variability in the data can be explained. We decided that bands later than 10th MNF band mostly include noise and hence can be discarded from analysis. After keeping 10 bands we next obtained the potential *Endmembers* using PPI algorithm. The

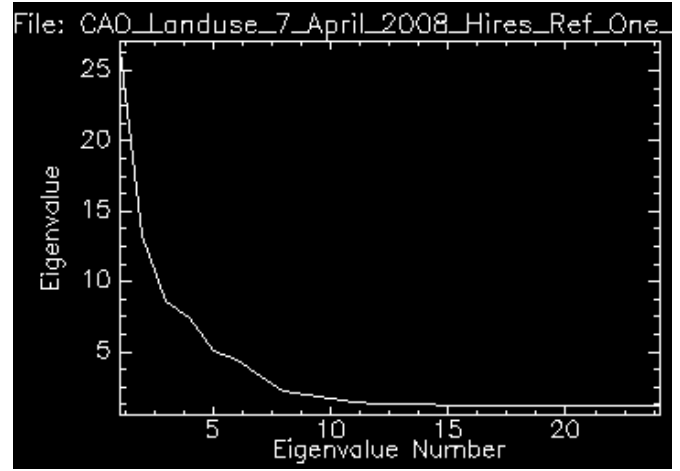


Fig. 3: Eigenvalue plot: 10 bands explain almost total variability in the dataset.

algorithm produced a total of 11 endmembers spectra as shown in Figure 4.

However, since we were only interested in classifying imagery into 4 classes- 1) Photosynthetic Vegetation (PV),

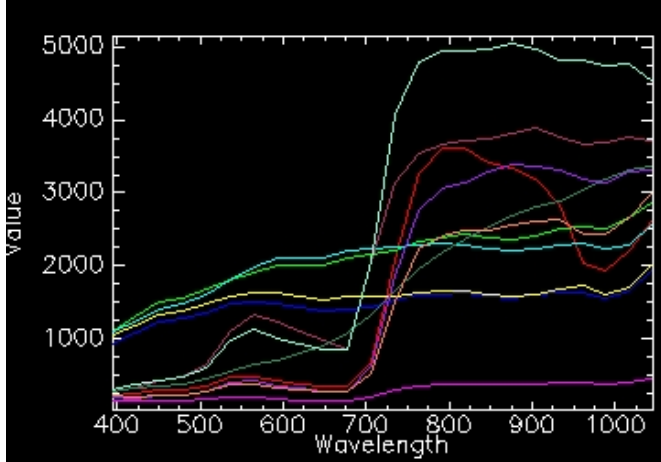


Fig. 4: All Endmembers obtained using the PPI algorithm.

2) Non-photosynthetic vegetation (NPV), 3) Bare Soil (BS) and 4) Shadow areas (S), we downsampled these endmember spectra to only those 4 spectra as shown in Figure 5.

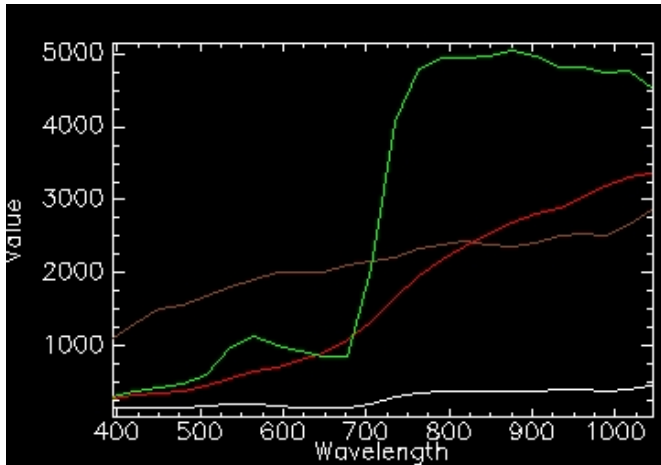


Fig. 5: Selected Endmembers: Green = PV, Red = NPV, Brown = Bare Soil, and White = Shadow.

These selected spectra then fed into linear-unmixing algorithm to obtain class abundance map as well as into SAM classification algorithm to obtain classification Map as shown Figure 6. We can see that the difference between PV and other end members can be easily visualized. However difficulty arises when trying to differentiate NPV from BS. The confusion maybe due to the high resemblance between those two spectra. The shadow regions are concentrated near the areas where the structures blocking sunlight are present. Such abundance maps can be used for gaining valuable insights about dominance of targets in the scene.

Again the selected endmembers are used to classify whole region based into our four classes based on spectral similarity with the pixel. The noise removed classified map for landuse-7 case based on spectral hourglass SAM algorithms is shown in Figure 7 (a). Same method was applied to the landuse-2 case imagery using the selected endmembers from landuse-7 case and the classmap is obtained as shown in Figure 7 (b). Visually

comparing- among classified pixels PV, NPV and Shadow classes are dominant in landuse-7 (degraded) case while PV and BS class are dominant in landuse-2 (conserved) case. So landuse-2 has higher proportion of Bare Soil pixels while landuse-7 have higher level of NPV. This can be attributed to the degradation of land which make it unfit for vegetation growth in case of landuse-7 which reflects in higher NPV levels. Again the distribution of PV is concentrated in central area of the scene while most of the area is unclassified in case of landuse-2 case, however the distribution of PV in case of landuse-7 case is sparse and uniform across the scene. This might be because we took the endmembers from degraded areas and used them for classifying conserved areas, thus the algorithm couldnt find relevant match for given threshold in conserved area and more area is unclassified.

To test the accuracy of such classification we selected 10 samples from each class using *stratified sampling* method and assessed how they appear in the scene vs how they are classified by the algorithm in both landuse-7 and landuse-2 cases. We used stratified sampling because it makes sure that samples for testing come from each classes and not a single class appear as majority and bias the assessment result. Also we choose *disproportionate* method for sampling since we are choosing only 10 samples from each class for testing no matter what their original population is. The confusion matrix for the landuse-7 classification is shown in Table I and for the landuse-2 is shown in Table II. We can see from the table that PV class has highest classification accuracy while NPV and shadow class are most confused between each other.

TABLE I: Confusion Matrix for Landuse-7 Classification

Actual / Predicted	PV	NPV	Bare Soil	Shadow
PV	9	1	0	0
NPV	2	8	0	0
BS	0	1	9	0
Shadow	0	1	0	9

TABLE II: Confusion Matrix for Landuse-2 Classification

Actual / Predicted	PV	NPV	Bare Soil	Shadow
PV	10	0	0	0
NPV	1	8	0	1
BS	0	1	9	0
Shadow	0	2	0	8

Using these two confusion matrices we can calculate the User's and Producer's accuracy for both classifications. These metrics are represented in the table Table III.

The classification results for Landuse-7 and Landuse-2 show high accuracy for Bare Soil and Shadow, with 100% user's accuracy (UA), indicating no commission errors. PV is well-classified, with high producer's accuracy (PA) (90%–100%) but some commission errors (UA: 81.82%–90.91%). NPV is the most challenging class, with lower UA (72.73%) and moderate PA (80%), suggesting misclassification with PV. Landuse-2 has a perfect PA for PV, while its Shadow class shows slightly higher misclassification compared to Landuse-7. Overall, classification is reliable, considering the simplicity of the algorithm used.

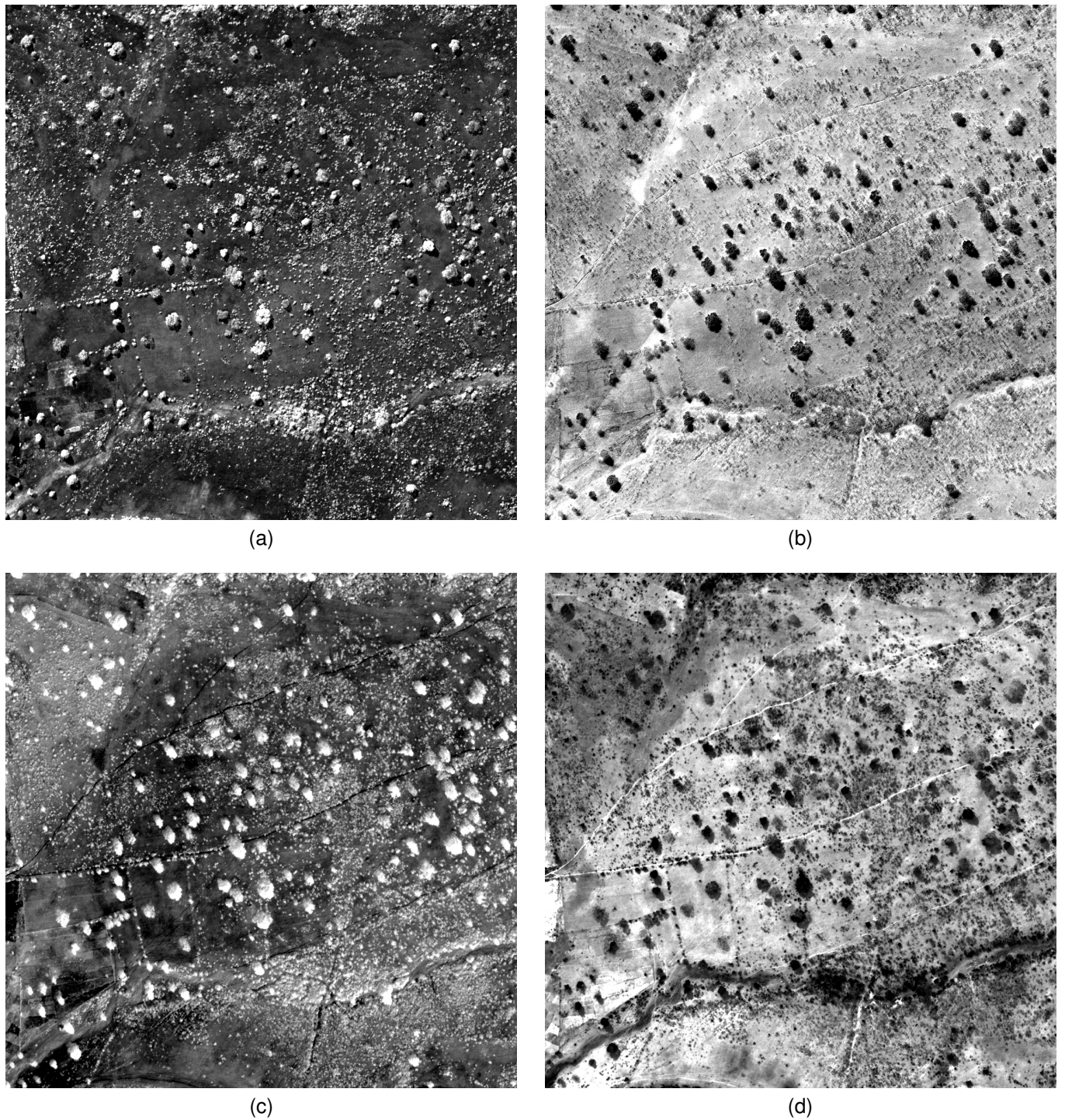


Fig. 6: Landuse-7 Abundance Map: (a) PV, (b) NPV, (c) Shadows, and (d) Bare Soil

TABLE III: User's and Producer's Accuracy for Landuse-7 and Landuse-2 Classifications

Class	Landuse-7		Landuse-2	
	Producer's Accuracy (%)	User's Accuracy (%)	Producer's Accuracy (%)	User's Accuracy (%)
PV	90.00	81.82	100.00	90.91
NPV	80.00	72.73	80.00	72.73
Bare Soil	90.00	100.00	90.00	100.00
Shadow	90.00	100.00	80.00	88.89

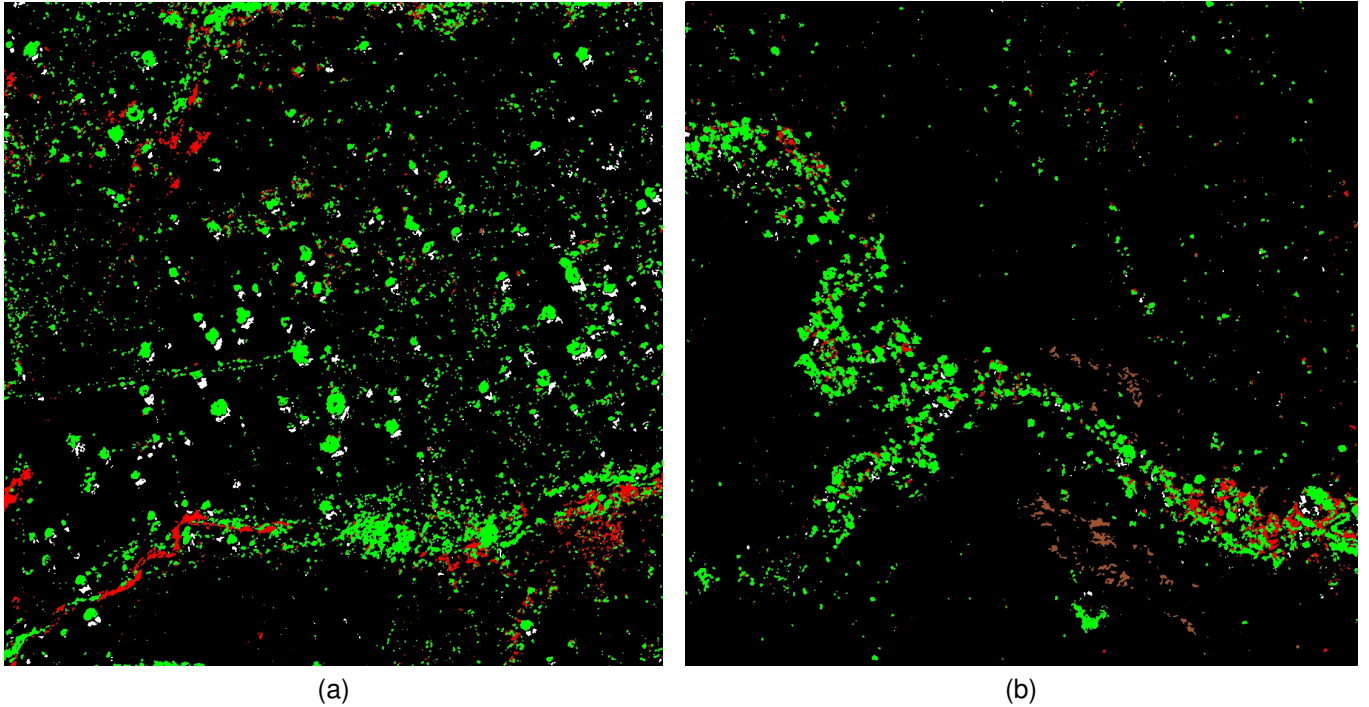


Fig. 7: (a) Landuse-7 (degraded) Classmap (b) Landuse-2 (conserved) Classmap.
Classes: Green = PV, Red = NPV, Brown = Bare Soil, White = Shadow, and Black = Unclassified.

IV. DISCUSSION AND CONCLUSION

Assessment of land degradation due to bush encroachment, lack of herbaceous matter and soil erosion using airborne hyperspectral remote sensing methods assists in policy making and guide in conservation practices. We used CAO hyperspectral imagery of two regions -1) Conserved area within Kruger National Park and 2) Degraded area outside the reserve area to determine the status of degradation and the indicators that explains the process. A simple yet elegant Spectral Mapping Algorithm (SAM) was used to classify the imagery into 4 classes- PV (photosynthetic vegetation), NPV (Non-photosynthetic vegetation), BS (Bare Soil) and Shadow areas. The classification results shows that the PV within the reserve were found to be accumulated to smaller portion and most of the area contains very sparse vegetation. Similarly the bare soil cover (BS) within reserved area is higher while it is comparatively lower in the communal areas. The NPV cover is relatively higher in degraded area compared to the communal area. Such widespread increase in NPV outside the reserve indicates a change in key landscape and soil properties such as loss of organic matter, which is an indicator of land degradation in such areas. This result is also consistent with the interpretation of Ashner *et. al.* [1]- NPV levels can be notable indicators of land degradation in communal areas. Again the assessment of the overall classification shows users accuracy above 70% and producers accuracy above 80% with negligible commission and a small omission error respectively. Comparatively speaking, NPV was the most challenging class while PV and shadow class were the easiest to classify. Overall the classification is dependable as it explains and gives insights

on the land degradation status within and outside of Kruger National Park.

REFERENCES

- [1] G. Asner and K. Heidebrecht, "Imaging spectroscopy for desertification studies: comparing aviris and eo-1 hyperion in argentina drylands," *IEEE Transactions on Geoscience and Remote Sensing*, vol. 41, no. 6, pp. 1283–1296, 2003.
- [2] L. Gao, X. Wang, B. A. Johnson, Q. Tian, Y. Wang, J. Verrelst, X. Mu, and X. Gu, "Remote sensing algorithms for estimation of fractional vegetation cover using pure vegetation index values: A review," *ISPRS Journal of Photogrammetry and Remote Sensing*, vol. 159, pp. 364–377, 2020. [Online]. Available: <https://www.sciencedirect.com/science/article/pii/S0924271619302783>
- [3] C.-I. Chang and A. Plaza, "A fast iterative algorithm for implementation of pixel purity index," *IEEE Geoscience and Remote Sensing Letters*, vol. 3, no. 1, pp. 63–67, 2006.
- [4] P. Ghamisi, N. Yokoya, J. Li, W. Liao, S. Liu, J. Plaza, B. Rasti, and A. Plaza, "Advances in hyperspectral image and signal processing: A comprehensive overview of the state of the art," *IEEE Geoscience and Remote Sensing Magazine*, vol. 5, no. 4, pp. 37–78, 2017.
- [5] F. Melgani and L. Bruzzone, "Classification of hyperspectral remote sensing images with support vector machines," *IEEE Transactions on geoscience and remote sensing*, vol. 42, no. 8, pp. 1778–1790, 2004.
- [6] J.-z. Wu, W.-d. Yan, W.-p. Ni, and H. Bian, "Feature extraction for hyperspectral data based on mnf and singular value decomposition," in *2013 IEEE International Geoscience and Remote Sensing Symposium - IGARSS*, 2013, pp. 1430–1433.
- [7] S. Shanmugam and P. SrinivasaPerumal, "Spectral matching approaches in hyperspectral image processing," *International Journal of Remote Sensing*, vol. 35, no. 24, pp. 8217–8251, 2014. [Online]. Available: <https://doi.org/10.1080/01431161.2014.980922>
- [8] R. G. Congalton, "A review of assessing the accuracy of classifications of remotely sensed data," *Remote Sensing of Environment*, vol. 37, no. 1, pp. 35–46, 1991. [Online]. Available: <https://www.sciencedirect.com/science/article/pii/003442579190048B>